DIRECT OBSERVATIONS OF LOW-ENERGY SOLAR ELECTRONS ASSOCIATED WITH A TYPE III SOLAR RADIO BURST*

L. A. FRANK and D. A. GURNETT

Department of Physics and Astronomy, The University of Iowa, Iowa City, Iowa 52240, U.S.A.

(Received 6 March; in revised form 7 July, 1972)

Abstract. A highly anisotropic packet of solar electron intensities was observed on 6 April 1971 with a sensitive electrostatic analyzer array on the Earth-orbiting satellite IMP-6. The anisotropies of intensities at electron energies of several keV were factors $\gtrsim 10$ favoring the expected direction of the interplanetary magnetic lines of force from the Sun. The directional, differential intensities of solar electrons were determined over the energy range 1–40 keV and peak intensities were $\sim 10^2$ cm^{-2} s^{-1} sr^{-1} eV^{-1} at 2–6 keV. This anisotropic packet of solar electrons was detected at the satellite for a period of 4200 s and was soon followed by isotropic intensities for a relatively prolonged period. This impulsive emission was associated with the onsets of an optical flare, soft X-ray emission and a radio noise storm at centimeter wavelengths on the western limb of the Sun. Simultaneous measurements of a type III radio noise burst at kilometric wavelengths with a plasma wave instrument on the same satellite showed that the onsets for detectable noise levels ranged from 500 s at 178 kHz to 2700 s at 31.1 kHz. The corresponding drift rate requires a speed of $\sim 0.15c$ for the exciting particles if the emission is at the electron plasma frequency. The corresponding electron energy of ~ 6 keV is in excellent agreement with the above direct observations of the anisotropic electron packet. Further supporting evidence that several-keV solar electrons in the anisotropic packet are associated with the emission of type III radio noise beyond $\sim 50R_\odot$ is provided by their time-of-arrival at Earth and the relative durations of the radio noise and the solar electron packet. Electron intensities at $E \gtrsim 45$ keV and the isotropic intensities of lower-energy solar electrons are relatively uncorrelated with the measurements of type III radio noise at these low frequencies. The implications of these observations relative to those at higher frequencies, and heliocentric radial distances $\lesssim 50R_\odot$, include apparent deceleration of the exciting electron beam with increasing heliocentric radial distance.

1. Introduction

The first firm observations of the presence of low-energy electrons, $E \sim 40$ keV, of solar origin in the interplanetary medium were reported by Van Allen and Krimigis (1965). The identification of these solar electron events was confirmed soon thereafter with an independent series of measurements at similar energies (Anderson and Lin, 1966). Subsequent detailed studies of the impulsive ejection of these electrons from the Sun have demonstrated the usefulness of such observations in contributing to our knowledge of solar flares and the interplanetary medium (Van Allen and Krimigis, 1965; Lin and Hudson, 1971, Lin, 1970) and of the magnetic field topology of the Earth's distant magnetosphere (Anderson and Lin, 1969; Van Allen, 1970). These results also provide a self-evident stimulus to extend the measurements to

* Research supported in part by the National Aeronautics and Space Administration under contracts NAS5-11039 and NAS5-11074 and grant NGL16-001-002 and by the Office of Naval Research under contract N000-14-68-A-0196-0003.

Solar Physics **27** (1972) 446–465.

lower energies. Recently observations of the energy spectrums of solar electrons extending down to 6 keV have been reported and have shown clearly that the differential intensities are increasing with decreasing energy over the energy range 6–300 keV (Anderson *et al.*, 1971). Ogilvie *et al.* (1971) also have interpreted several of their observations of lower energy electrons, 0.34–9 keV, in the interplanetary medium near the Earth as the low-energy segment of the solar electron spectrum.

The frequent association of type III solar radio noise bursts with impulsive, low-energy solar electron ($E \gtrsim 40$ keV) events as measured at the Earth has been noted previously by Lin (1970). Type III solar radio noise bursts are characterized by an emission frequency which decreases with increasing time. The frequency range of type III radio noise is large, extending from frequencies of several hundred mHz (Kundu, 1965) down to frequencies of a few tens of kHz as discussed in our present paper. Wild (1950) first proposed that the frequency variation of these radio noise bursts is caused by the motion, outward from the Sun, of a disturbance which was attributed to charged particles of solar origin. These charged particles were presumed to generate radiation at frequencies at or near the electron plasma frequency of the solar corona. The decreasing plasma frequency arising from decreasing electron densities with increasing heliocentric radial distances, together with the nearly uniform outward motion of the exciting disturbance, provided a plausible explanation of the observed frequency variations. Subsequent investigations of the detailed character of type III noise bursts have contributed strong support for the major features of this hypothesis (cf. Kundu, 1965).

Numerous estimates of the speeds of the charged particles exciting the type III emissions have been reported. Estimates of the particle speeds from the frequency drift rates by invoking the Baumbach-Allen model of the solar corona yield speeds in the range 0.1–0.3c (c, speed of light) (Wild, 1950). Directional measurements of the apparent position of the source of type III noise as it moves outward from the Sun indicate higher speeds ranging from 0.2–0.8c and averaging approximately 0.45c (Wild *et al.*, 1959). Recently observations of the type III solar radio noise bursts down to a frequency of 540 kHz have been interpreted in terms of particle speeds ranging from 0.2–0.6c and averaging 0.37c (Fainberg and Stone, 1970; 1971a). These speeds are similar to those of the low-energy solar electrons frequently observed to accompany these radio noise bursts (40 keV corresponds to an electron speed of 0.37c).

On 6 April 1971 a solar X-ray flare and a type III solar radio noise burst were observed with instrumentation on the eccentric-orbiting satellite IMP-6. The type III solar radio noise burst was detected down to a frequency of 31 kHz. A highly anisotropic packet of low-energy solar electron intensities arrived at the satellite approximately 5000 s after the onset of the solar flare. This packet of solar electron intensities was observed for 4200 s. Maximum differential intesities of these solar electrons were in the energy range 2–6 keV. The frequency drift rate of the type III radio noise at frequencies below 178 kHz also indicated an average particle speed corresponding to that of a 6-keV electron. This paper presents our simultaneous observations of

these solar electron intensities and of the type III solar radio burst and explores their interrelationships.

2. Observations

Our measurements of low-energy solar electrons and of solar radio noise reported here were gained with the University of Iowa electrostatic analyzer arrays and plasma wave instrumentation on the Earth-orbiting satellite IMP-6. IMP-6 (Explorer 43) was launched on 13 March 1971 into an orbit with initial perigee and apogee geocentric radial distances 6620 km and 211 250 km, respectively, inclination 28.6° and period 99.4 h. During the series of observations presented here the spacecraft was located at 160000–195000 km geocentric radial distances and substantially upstream from the Earth's magnetosheath. The corresponding angle between the Earth-to-Sun and Earth-to-satellite vectors was $\lesssim 20°$.

The Low Energy Proton and Electron Differential Energy Analyzer, or LEPEDEA, provides measurements of the differential energy spectrums and angular distributions of proton and electron intensities over the energy range $10 \leqslant E \leqslant 40000$ eV. These electrostatic analyzers are capable of simultaneous determinations of proton and electron intensities within each of 16 energy bandpasses. Threshold intensities are approximately 4 and 0.2 protons or electrons $\mathrm{cm}^{-2}\,\mathrm{s}^{-1}\,\mathrm{sr}^{-1}\,\mathrm{eV}^{-1}$ at 1 keV and 40 keV, respectively. The axes of the fields-of-view of the LEPEDEA are directed normal to the satellite spin axis. This spin axis is perpendicular to the ecliptic plane, and the spin rate is approximately 5 revolutions per minute. The dimensions of the nearly rectangular fields-of-view are 8° in the ecliptic plane and 30° in a plane containing the spin axis and hence perpendicular to the ecliptic. The cycling of the analyzer plate voltages is slaved to the spacecraft clock. A relatively complex series of stepped voltages is applied to the analyzer plates. The duration of each energy step is 0.32 s and the entire series of 128 energy steps in the instrument cycle spans a period of 40.96 s. The responses of the analyzers are sampled with digital accumulators for 0.32 s at each of the above energy steps. Corresponding directions for the axes of the fields-of-view of the LEPEDEA are determined for each sampling period from the spacecraft optical aspect information. During each instrument cycle of 40.96 s, 248 measurements of proton and electron intensities, together with 4 responses of a thin-windowed Geiger-Mueller tube, are telemetered. The Geiger-Mueller tube has a conical field-of-view with full angle 30°. The axis of this field-of-view is also directed perpendicular to the spacecraft spin axis and thus lies parallel to the ecliptic plane. This detector is sensitive to electrons $E \gtrsim 45$ keV and protons $E \gtrsim 650$ keV within its field-of-view. Further information concerning the LEPEDEA instrument has been published previously (Frank, 1967; Frank *et al.*, 1969).

The plasma wave and radio noise antenna arrays on IMP-6 consist of two long dipole antennas (approximately 100 meters tip-to-tip when fully extended) for electric field measurements and three orthogonal loop antennas for magnetic field measurements. The electric antennas are positioned perpendicular to the spin axis of the spacecraft. During the period of observations reported here the electric antennas

were extended to a tip-to-tip length of 42 m. The University of Iowa radio noise instrumentation comprises two 16-channel frequency spectrum analyzers, one for an electric antenna and the other for a magnetic antenna. These spectrum analyzers covered the frequency range from 20 Hz to 200 kHz with four channels per decade of frequency. The responses of the 16 frequency channels for both spectrum analyzers are telemetered once each 5.12 s. Due to the larger dimensions of the electric antennas relative to the loop antennas, the electric antennas are substantially more sensitive than the magnetic antennas for detecting electromagnetic waves. Correspondingly all observations of radio noise intensities as presented herein have been gained from an electric antenna, although similar measurements are available from a magnetic antenna with higher threshold levels.

A. OVERALL SIGNATURE OF THE LOW-ENERGY SOLAR ELECTRON EVENT

Measurements of the energy fluxes of solar X-rays within the wavelength range 2–12 Å as obtained from the responses of the thin-windowed Geiger-Mueller tube as it viewed the Sun are shown in the top panel in Figure 1. Two X-ray events are evident during these 12 h of observations, one with peak fluxes at 0950 UT and the other at 1410 UT. The first X-ray emission commencing at approximately 0935 UT and attaining peak energy fluxes of 0.02 erg cm^{-2} s^{-1} is followed by the later arrival of low-energy electron intensities well above our instrument thresholds as shown in the bottom three panels of Figure 1. The burst of solar X-rays and the emission of low-energy electrons can be associated almost certainly with solar flare activity of importance −B and beginning 0935 UT in McMath Plage Region 11221 at location S19°, W80° (*NOAA*, 1971).

Our major interest here is directed toward the observations of low-energy electron intensities with $E > 45$ keV, $5.5 \leqslant E \leqslant 6.3$ keV and $3.5 \leqslant E \leqslant 4.1$ keV as summarized in Figure 1. The inset in the left-hand side of the second panel defines the angular sectors in the ecliptic plane for this series of observations. The angular coordinate φ_{SE} is the spacecraft-centered solar ecliptic longitude of the axis of the instrument field-of-view. The increases of intensities due to the arrival of solar electrons within each of the energy ranges shown in Figure 1 are a factor $\gtrsim 10$ above the instrument threshold or the interplanetary background. Maximum intensities of electrons within the energy ranges $E > 45$ keV, $5.5 \leqslant E \leqslant 6.3$ keV and $3.5 \leqslant E \leqslant 4.1$ keV were $\sim 10^3$ cm^{-2} s^{-1} sr^{-1}, 40 cm^{-2} s^{-1} sr^{-1} eV^{-1} and 10^2 cm^{-2} s^{-1} sr^{-1} eV^{-1}, respectively. The Geiger-Mueller tube responses have been identified as electrons ($E > 45$ keV) unambiguously via observations of the same event at similar energies with Explorers 33 and 35 (Van Allen, private communication). A relatively prolonged period of weak anisotropy of electron ($E > 45$ keV) intensities occurs near the onset of the event at 1110 UT through 1220 UT and is coincident with the appearance of a 'packet' of lower- energy electron intensities with energies of the order of several kiloelectron volts (see bottom two panels of Figure 1, same time interval). As demonstrated in our later discussion, these lower-energy electron intensities are highly anisotropic during this period. The corresponding anisotropy of electron intensities with $E > 45$ keV, defined here as the

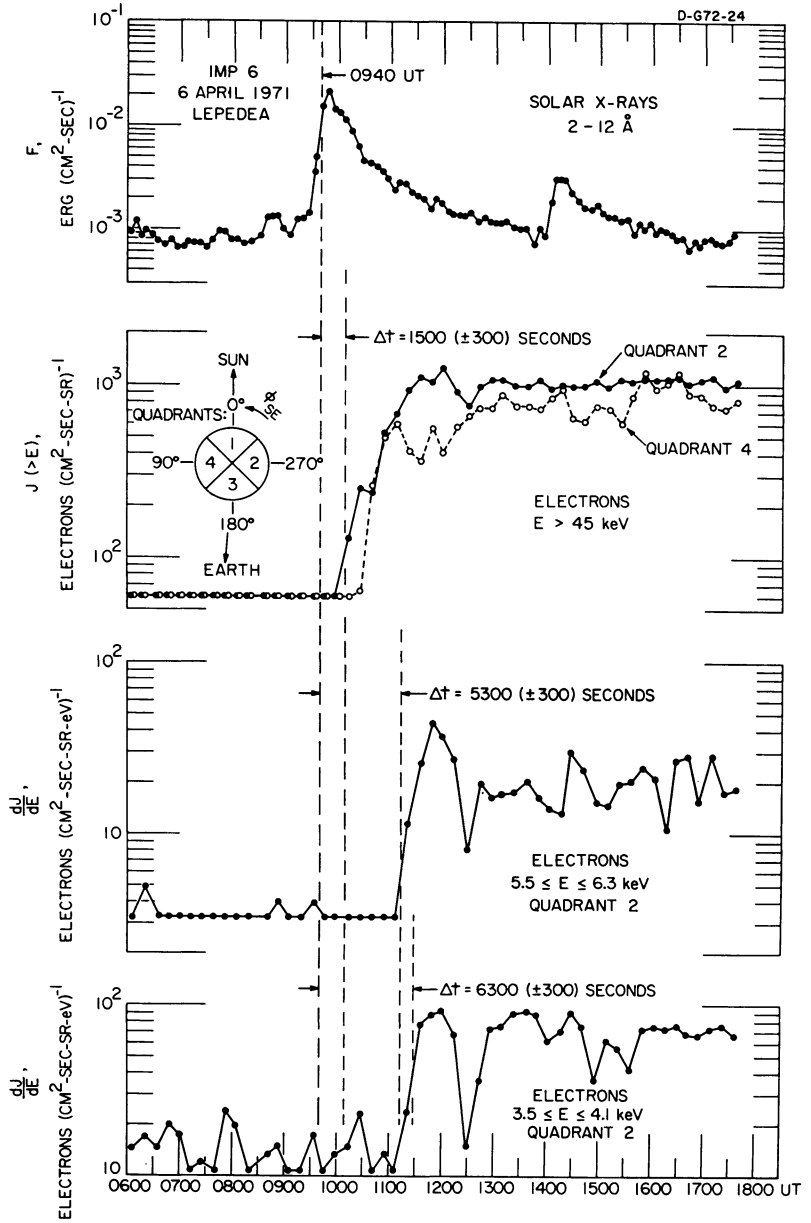

Fig. 1. Observations of the impulsive emission of low-energy solar electrons with an electrostatic analyzer on the satellite IMP-6. Energy fluxes of solar X-rays in the wavelength range 2–12 Å are shown in the top panel and electron intensities in three selected energy ranges are shown in the bottom panels. The impulsive emission of these electron intensities was associated with the onsets of an optical flare at 0935 UT and of a radio noise storm at centimeter wavelengths at 0940 UT, 6 April 1971. The coordinate φ_{SE}, shown in the inset of the second panel, is the solar ecliptic longitude of the direction of the detector's field-of-view in satellite-centered coordinates.

ratio of intensities in quadrant 2 to those observed in quadrant 4, is ~2.5.

Perhaps one of the most striking features of the observations of Figure 1 is the increasing time of arrival of solar electron intensities at the Earth with decreasing electron energies. In order to determine the propagation times for these solar electrons over the path from Sun to Earth we have chosen the injection time as 0940 UT on the basis of a concurrent onset of a major radio noise storm observed at high frequencies by ground-based solar radio observatories (*NOAA*, 1971). This time for the start of solar electron emission is in tolerable agreement with the onset of the optical flare as noted above and with the profile of solar X-ray fluxes reported here. However, for the calculation of electron propagation times, our uncertainties in the determination of observed arrival times are approximately ± 5 min and probably represent equal or greater inaccuracies in determining the propagation times than the above adoption of an ejection time from solar observations.

A summary of the observed propagation times from Sun to Earth for solar electrons in the three energy ranges shown in Figure 1 are summarized in Table I. These propagation times are the intervals bracketed by our reference time, 0940 UT, and the time at which measurable intensities of electrons within the corresponding energy ranges were observed. The correction for the light propagation delay to Earth has been included. The calculated propagation times for electrons of each energy, assuming pitch angle $\alpha = 0°$ along a smooth Archimedean spiral, are also given in Table I. The average solar wind velocity used in determination of the length of the interplanetary magnetic field line was 350 km s^{-1} (Ogilvie, private communication; *NOAA*, 1971).

TABLE I

Comparison of observed delays in electron arrival times with calculated delays for a smooth Archimedean spiral ($V_S = 350$ km s^{-1})

Electron energy	Observed propagation time[a] (s)	Calculated propagation time (s)	Ratio of propagation times observed / calculated
3.8 keV	6800 ($\pm$300)	4900	1.38 ($\pm$0.08)
5.9 keV	5800 ($\pm$300)	3950	1.47 ($\pm$0.08)
45 keV	2000 ($\pm$300)	1510	1.33 ($\pm$0.20)

[a] Includes correction for light propagation delay to Earth.

The ratios of the observed propagation times to those calculated in the above manner are ~1.4. Although the energies of the solar electrons differ by at least an order of magnitude this ratio is constant within observational errors. This result indicates that these solar electrons were ejected simultaneously at all energies into the interplanetary medium and that the longer propagation times relative to the computed values reflect (a) increased path length due to irregularities in the interplanetary mag-

netic field and/or (b) electron pitch angles $\alpha > 0°$. We will not be able to resolve these two possibilities with the present series of observations.

B. ANGULAR DISTRIBUTIONS OF SOLAR ELECTRON INTENSITIES

The intensities of low-energy solar electrons within the energy range $5.5 \leqslant E \leqslant 6.3$ keV viewed within quadrants 2 and 4 in the ecliptic plane are shown in Figure 2. Quadrants 2 and 4 span ranges of solar ecliptic longitudes of 225–315° and 45–135°, respectively. The threshold intensity for the instrument at the temporal resolution shown in Figure 2 is 3.3 electrons $cm^{-2}\ s^{-1}\ sr^{-1}\ eV^{-1}$. The anisotropies of intensities observed during 1110–1220 UT ranged from factors of 3 to $\gtrsim 10$, always in favor of quadrant 2. Nearly isotropic solar electron intensities were observed at 1240 UT, 5400 s after the first detection of the highly anisotropic solar electron packet. These nearly isotropic intensities were present at the satellite position for at least five hours during the period 1240–1740 UT.

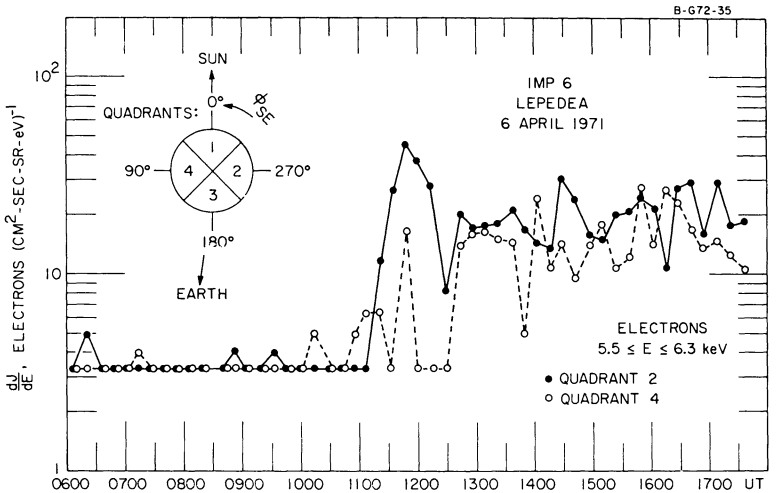

Fig. 2. Directional, differential intensities of solar electrons ($5.5 \leqslant E \leqslant 6.3$ keV) as functions of time for the angular quadrants 2 and 4. A highly anisotropic packet of solar electrons was detected at 1110 to 1220 UT and was followed by a prolonged period of relatively isotropic intensities beginning at 1240 UT.

A more detailed examination of the angular distributions of solar electron intensities in the anisotropic packet is presented in Figure 3. The angular distributions of electron intensities in the energy range $3.5 \leqslant E \leqslant 4.1$ keV are strongly peaked at $\varphi_{SE} \simeq 300°$ with an apparent beam width at half-maximum intensities of $\sim 60°$. This width may be the signature of (a) the pitch angle distributions of the solar electron intensities and/or (b) fluctuations in the directions of the solar electron velocity vectors as viewed from the spacecraft during the period of observations, which are effected by temporal variations of the direction of the interplanetary magnetic field. Vertical

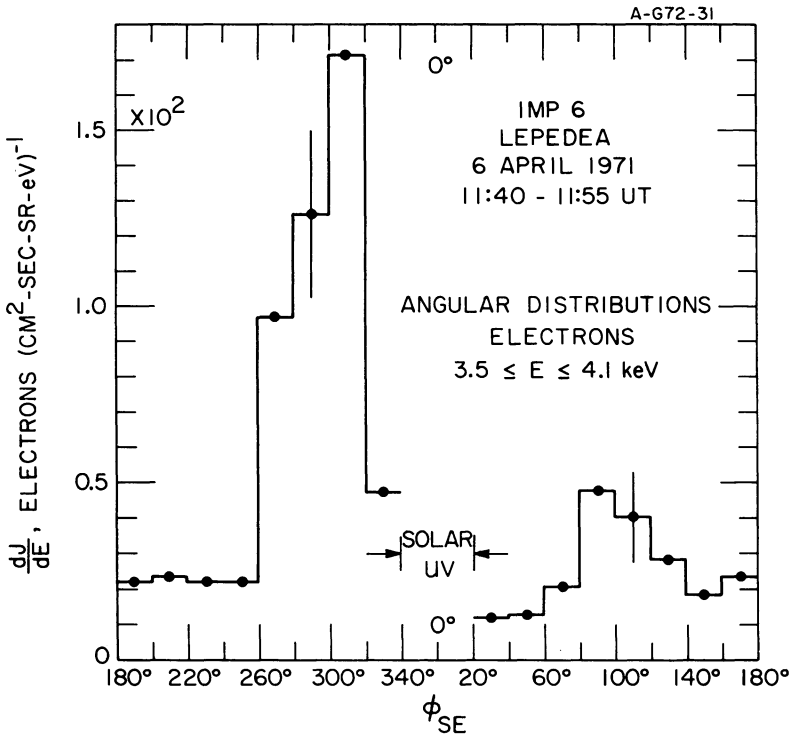

Fig. 3. Angular distributions of solar electron intensities ($3.5 \leqslant E \leqslant 4.1$ keV) within the anisotropic packet. The solar electron intensities are strongly peaked at $\varphi_{SE} \simeq 300°$ near the expected direction of the Archimedean spiral of the interplanetary magnetic lines of force.

lines through the data points indicate the standard deviation for the counting statistics. The major peak of electron intensities at $\varphi_{SE} \simeq 300°$ occurs near the expected angle for the computed Archimedean spiral line, which is 311° for a solar wind velocity of 350 km s^{-1}. It is highly improbable that the singly-peaked angular distributions shown in Figure 3 can be interpreted in any other manner than as a beam of electron intensities directed parallel to the interplanetary magnetic field. Future comparisons with simultaneous magnetic field measurements will provide more information as to the detail of the angular distributions of solar electron intensities, such as the apparent width as reported here. No determinations of electron intensities in the angular segment with width 40° and centered in the solar direction, $\varphi_{SE} = 0°$, are given in Figure 3 due to small, but significant contamination of the instrument responses by solar ultraviolet fluxes. However, the maximum electron intensities observed in these directions are $\lesssim 10^2$ electrons cm^{-2} s^{-1} sr^{-1} eV^{-1}. The minor peak of electron intensities centered at $\varphi_{SE} \simeq 100°$ is most likely attributable to either solar electrons which have been reflected by the Earth's bow shock or magnetosheath electrons propagating upstream in the interplanetary medium. These peak intensities

are less by factors ~ 4 relative to those observed at $\varphi_{SE} \simeq 300°$ for the packet of solar electrons propagating outward from the Sun along the interplanetary spiral.

C. ENERGY SPECTRUMS OF SOLAR ELECTRON INTENSITIES

In order to determine the energy spectrums of the solar electrons attributable to impulsive emission associated with the flare we must establish first the background interplanetary electron intensities in the energy range of present interest. The differential energy spectrums of electron intensities prior to the occurrence of the transient

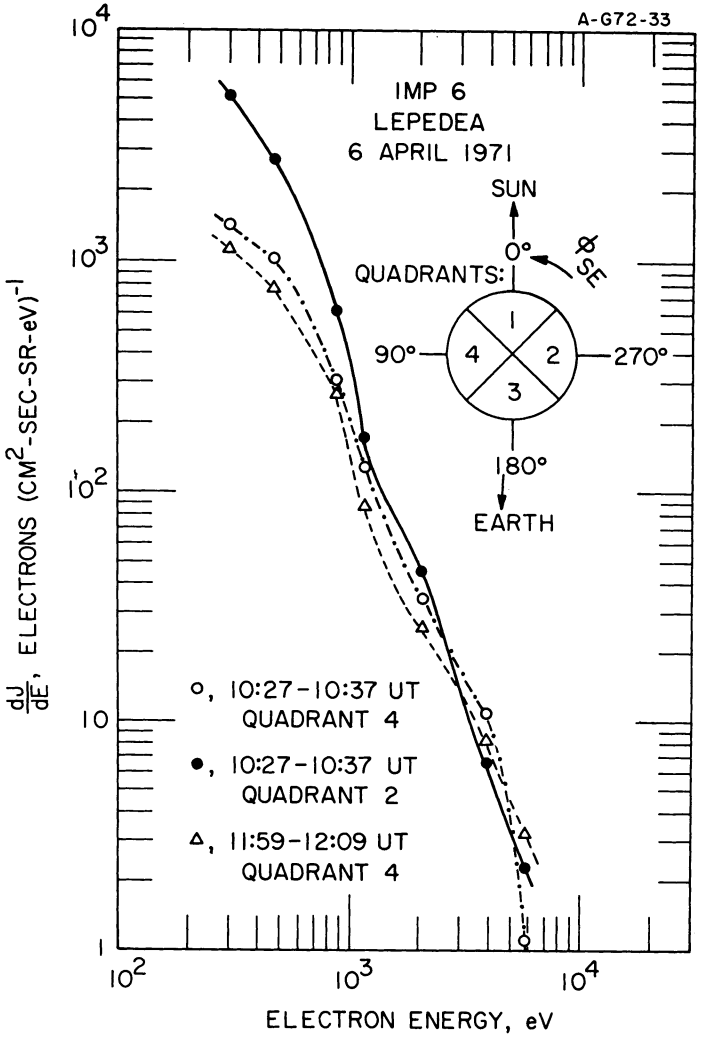

Fig. 4. Directional, differential energy spectrums of electron intensities prior to the arrival of the anisotropic solar electron packet (open circles, quadrant 4, and solid circles, quadrant 2) and during the presence of the anisotropic packet but in quadrant 4 (triangles) opposite to the direction of arrival of the solar electrons. The anisotropies of intensities at electron energies $\lesssim 1$ keV are related to the heat flux of solar wind electrons.

solar electron intensities are shown in Figure 4 for quadrants 2 (solid circles) and 4 (open circles). Differential intensities increase with decreasing electron energy over the energy range $0.30 \leqslant E \leqslant 6$ keV given in Figure 4. The intensities are approximately isotropic at energies $\gtrsim 1$ keV. The anisotropy of intensities evident for electron energies $\lesssim 1$ keV is the direct signature of the heat flux of the ambient solar wind electrons (cf. Montgomery *et al.*, 1968). Also shown in Figure 4 is an example of the energy spectrums of electron intensities in quadrant 4 (triangles) *during* the period of observations of the highly anisotropic packet of transient solar electron intensities detected

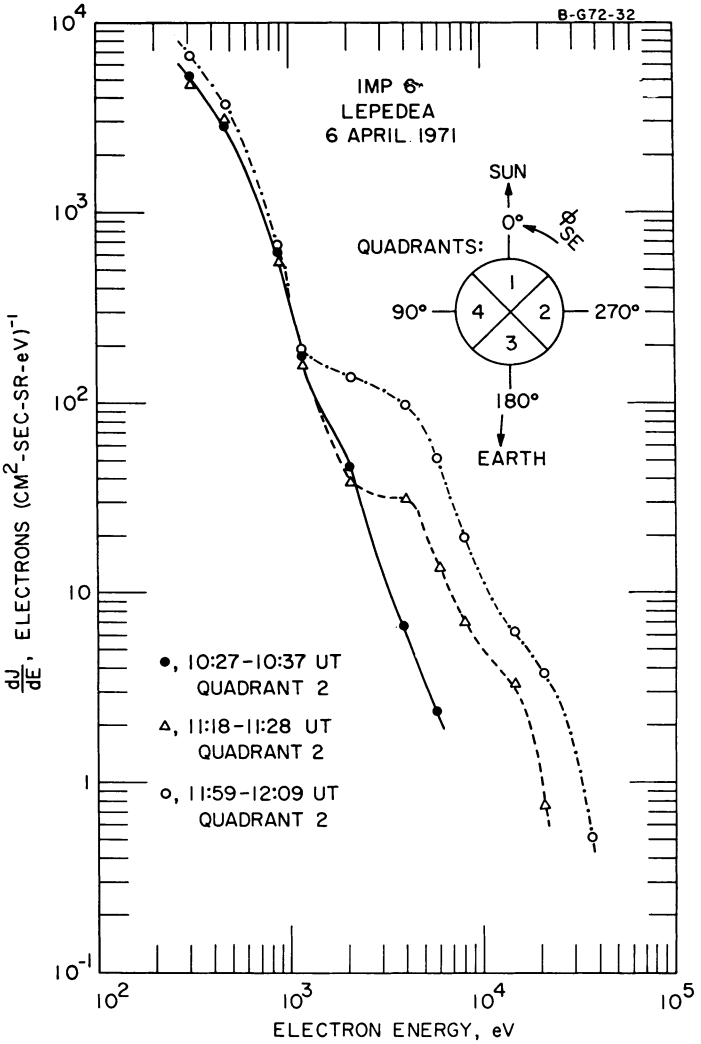

Fig. 5. Directional, differential energy spectrums of electron intensities in quadrant 2 prior to the arrival of the anisotropic packet (solid circles), at the leading edge of this solar electron packet (triangles), and during the period of peak intensities for the packet (open circles).

in quadrant 2 (see also Figure 1). The electron spectrums in quadrant 4 just prior to and during the transient event are identical within observational errors.

On the other hand, large increases of electron intensities with energies $\gtrsim 1$ keV are observed in quadrant 2 with the appearance of the transient solar electron packet. The pre-event electron spectrum of Figure 4 (solid circles) is compared to two solar electron spectrums within the anisotropic packet in Figure 5. These two spectrums at 1118–1128 UT (triangles) and 1159–1209 UT (open circles) as shown in Figure 5 demonstrate clearly that electrons with energies ~ 2 keV arrive later than those with energies ~ 4keV and that the ambient solar wind spectrum is substantially unaffected at electron energies $\lesssim 1$ keV. A straightforward subtraction of the ambient electron spectrum from those observed during the presence of the transient solar electron intensities allows a relatively simple determination of the energy spectrums of transient electron intensities. These energy spectrums of solar electrons within the anisotropic packet are shown in Figure 6. The vertical bars through the data points denote our assessment of the combined errors in the subtraction of ambient intensities and the standard deviations for the counting statistics. It is noteworthy that the electron

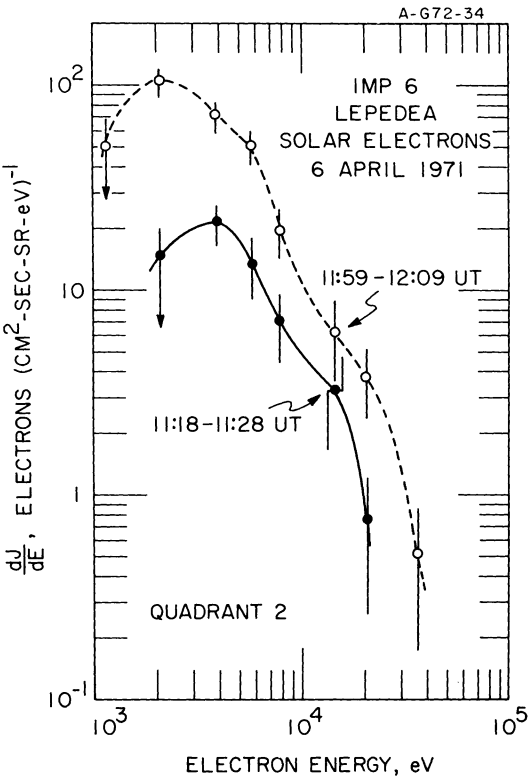

Fig. 6. Directional, differential spectrums of solar electron intensities at the leading edge (solid circles) and at peak intensities (open circles) for the anisotropic packet. Peak intensities were $\sim 10^2$ cm^{-2} s^{-1} sr^{-1} eV^{-1} at electron energies $\sim$ 2–6 keV.

spectrums increase in overall intensities and display a decreasing energy for peak differential intensities with increasing time in the leading edge of the packet. Peak differential intensities are $\sim 10^2$ cm^{-2} s^{-1} sr^{-1} eV^{-1} at $\sim$2keV.

The total number of electrons and the total energy within the anisotropic solar electron packet can be coarsely estimated by assuming a solid angle of ~ 1 sr for the electron beam at the Earth's orbit as viewed from the Sun. These estimates for the total number and energy of solar electrons are $\sim 5 \times 10^{35}$ electrons and 3×10^{27} ergs. The heliocentric radial depth of the packet at the Earth's orbit is $\sim v \cos\theta \, \Delta t$, where v is the average electron velocity, θ is the inclination of the interplanetary field lines to the Sun-to-Earth line, and Δt is the duration of the event as seen at the spacecraft. This radial depth is ~ 0.5 AU. Peak energy fluxes along the interplanetary lines of force and attributable to these transient solar electron intensities are $\sim 4 \times 10^{-3}$ erg cm^{-2} s^{-1}, and are within factors of ~ 2 of the average heat fluxes due to ambient interplanetary solar wind electrons (cf. Montgomery *et al.*, 1968). The electron densities in the anisotropic packet are $\sim 10^{-4}$ cm^{-3} within the energy range $1 \lesssim E \lesssim 40$ keV and $\lesssim 10^{-6}$ cm^{-3} for electron energies $\gtrsim 45$ keV. If the differential energy spectrums of Figure 6 are approximated with a Boltzmann distribution the corresponding temperatures are similar to those reported by Drake (1971) as deduced from observations of solar X-ray bursts in the energy range 1–50 keV. Further studies of a series of these low-energy solar electron events beyond our present initial report should provide additional information concerning the emission of solar electrons and their subsequent propagation in the interplanetary medium.

D. ASSOCIATED TYPE III SOLAR RADIO NOISE BURST

Observations of the type III radio noise event associated with the impulsive ejection of solar electrons as discussed above are summarized in Figure 7. This type III radio noise burst, shown as shaded areas in the four bottom panels of Figure 7, comprises two distinct bursts with onset times in 178-kHz channel at 0920 UT and 0948 UT, respectively. The increasing delay of observation with decreasing frequency, characteristic of type III radio noise emission, is clearly evident for each of these bursts. Type III radio noise was not detected at 16.5 kHz which is the next lowest frequency channel below the 31.1-kHz channel.

The first, lesser type III radio burst commencing at 0920 UT, as detected in the 178-kHz frequency channel, occurs substantially before the onset of the optical flare and solar X-ray emission at approximately 0935 UT. This radio burst can be associated with a radio noise storm observed at higher frequencies beginning at 0914 UT (*NOAA*, 1971). Due to the above sequence of events it is believed that this lesser noise burst is not associated with the emission of the low-energy solar electrons. The second and most intense type III burst beginning at 0948 UT in the 178-kHz channel commences at ~ 500 s after the onset of a high-frequency solar radio noise event at 0940 UT (*NOAA*, 1971). The relative magnitude of this radio noise burst and its juxtaposition in time relative to those of the centimeter solar radio noise, the optical flare and the X-ray emission are the features which we judge are sufficient to associate

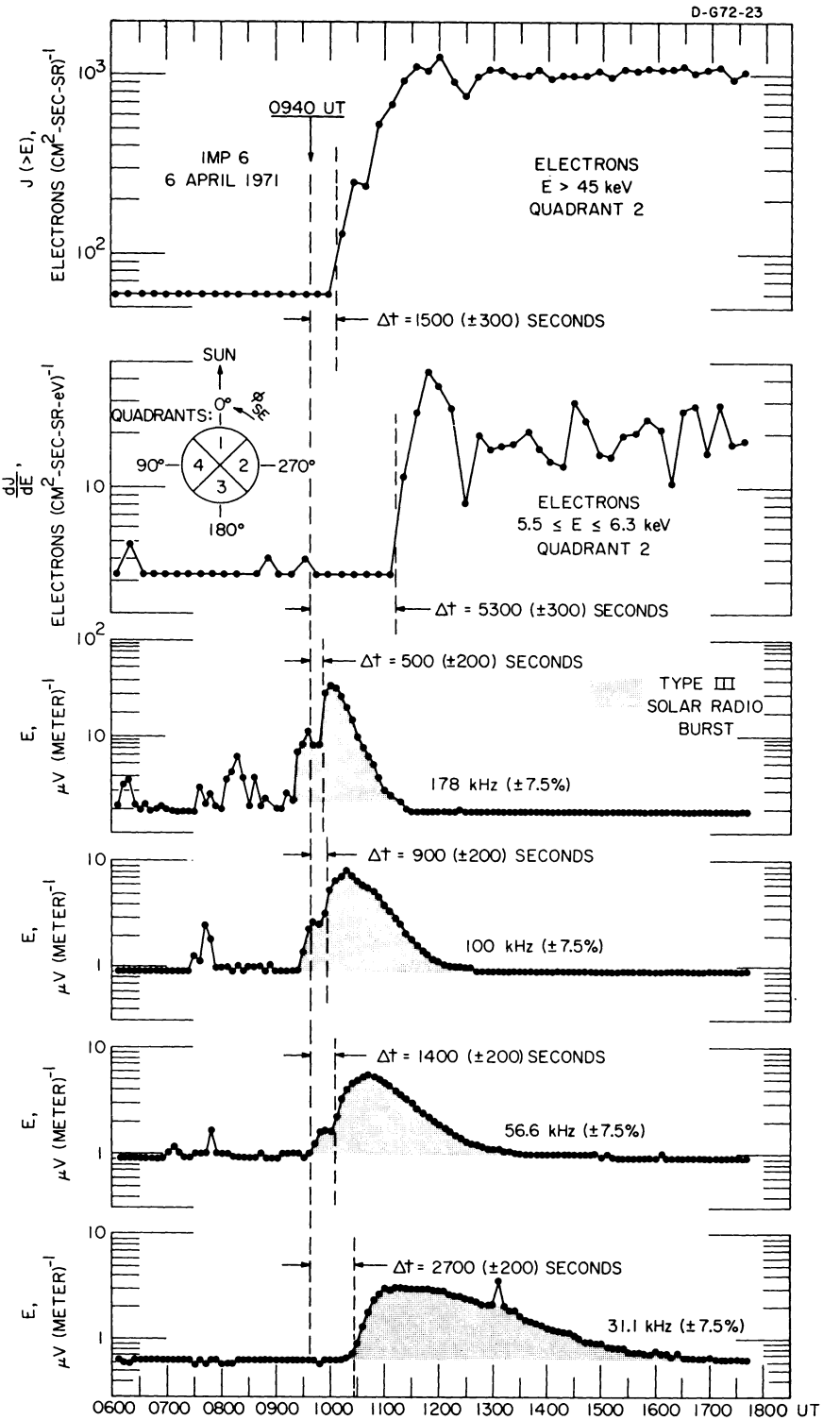

Fig. 7. (see for caption page 459.)

this second radio burst with the events accompanying the flare. The delays for the onsets of detectable radiation at the four frequencies shown in Figure 7, as measured from 0940 UT, are 500, 900, 1400 and 2700 s at 178, 100, 56.6 and 31.1 kHz, respectively, within the observational uncertainties of ± 200 s. These drift rates allow an estimate of the speed of the exciting particles if it is assumed that the radio noise is generated at the plasma frequency and that these particles are travelling radially outward from the Sun. For a number density of 5 cm^{-3} at 1 AU as observed with a solar wind ion detector on IMP-6 (Ogilvie, private communication) and with the inverse square law for the density as a function of heliocentric radial distance, the corresponding average speed for the exciting particles is $0.15c$. This speed corresponds to an electron energy of ~ 6 keV which is in excellent agreement with the direct observations of solar electrons within this energy range as reported here. Observations of solar electron intensities in the energy ranges $5.5 \leqslant E \leqslant 6.3$ keV and $E > 45$ keV are given in the upper two panels of Figure 7 for comparison with the radio noise measurements. The relatively rapid arrival of solar electrons with energies > 45 keV (speed, $> 0.39c$) with a delay of only ~ 1500 s clearly demonstrates that electrons of these energies cannot be responsible for the type III solar radio noise generated at these low frequencies. Due to the relatively steep plasma density gradient nearer to the Sun the duration of the radio noise at the higher frequencies reported here should provide an approximate measure of the time interval during which the exciting particles intersected the corresponding heliocentric radial distance if the radio noise is generated at the plasma frequency. As shown in Figure 7 the observed durations of the 178-kHz radio noise and of the anisotropic solar electron packet are ~ 5400 s and 4200 s, respectively. This result provides further evidence that the anisotropic solar electron packet is exciting the low-frequency type III solar radio noise. On the other hand, it is evident from the observations shown in Figures 2 and 7 that the nearly isotropic intensities of low-energy solar electrons detected for a prolonged period after 1240 UT persist at relatively constant intensities throughout the decrease of radio noise and hence are largely uncorrelated with the temporal behavior of the type III solar burst at low frequencies.

3. Discussion

Direct observations of the impulsive ejection of a highly anisotropic, low-energy solar electron packet which was accompanied by a type III solar radio noise burst detected simultaneously with instrumentation on the satellite IMP-6 have been examined here. These events were associated with a solar flare commencing at 0935 UT,

Fig. 7. Comparison of simultaneous observations of type III solar radio noise at low frequencies with the measurements of low-energy solar electrons at 1 AU. The electron plasma frequency was ~ 19.9 kHz at 1 AU. The onset of 45-keV electron intensities occurs too rapidly to be associated with the generation of type III radio noise at these low frequencies. On the other hand, the time-of-arrival, speed and duration of the lower-energy, anisotropic packet of solar electron intensities at 1110–1220 UT are in excellent correlation with those of the type III radio noise burst if the radio noise is generated at the electron plasma frequency.

6 April 1971, on the western limb of the Sun. The duration of the anisotropic solar electron event, as measured at the satellite position, was 4200 s. This event was followed by a prolonged period, $\gtrsim 5$ h, during which the intensities were approximately isotropic. Angular distributions of low-energy electron intensities in the anisotropic packet were strongly peaked at $\varphi_{SE} \simeq 300°$, at or near the expected direction of the interplanetary magnetic field. Anisotropies of intensities were typically factors of $\gtrsim 10$ favoring the direction of propagation from the Sun. Maximum directional, differential intensities were $\sim 10^2$ cm^{-2} s^{-1} sr^{-1} eV^{-1} at 2–6 keV. The energy spectrums of electron intensities within the highly anisotropic packet were determined for the energy range 1–40 keV. A study of the propagation times for the low-energy solar electrons within the energy range 3.5–45 keV demonstrated that the ratio of the observed times to corresponding times calculated for motion parallel to a smooth Archimedean spiral was ~ 1.4 and was independent of electron energy. This result indicates that these solar electrons were directly injected into the interplanetary medium without a substantial storage period near the Sun and that the delay is probably attributable to irregularities in the interplanetary magnetic field and/or electron pitch angles $\alpha > 0°$. The observed Sun-to-Earth propagation times were 6800, 5800 and 2000 s for electron energies of 3.8, 5.9 and ~ 45 keV, respectively, within overall observational errors of ± 500 s.

Simultaneous measurements of solar radio noise at low frequencies in the range 31.1–178 kHz revealed that a type III solar radio burst was associated with this flare. The delay times for detection of this radio noise at levels above the threshold of the receiver increased with decreasing frequency. These delays were 500, 900, 1400 and 2700 s at 178, 100, 56.6 and 31.1 kHz, respectively, within an accuracy of ± 200 s. Both the propagation times of the solar electrons and the delays for the type III radio noise are relative to the onset of the solar radio noise storm at 0940 UT as reported by ground-based observatories at centimeter wavelengths. The measured drift rate of the type III radio burst at low frequencies, together with a solar wind density of 5 cm^{-3} at 1 AU, can be used to estimate the speed of the exciting particles. This speed is $0.15c$. The corresponding electron energy is 6 keV which is in excellent agreement with the energies at peak differential intensities in the anisotropic solar electron packet.

This close association of the type III radio burst at low frequencies and the anisotropic solar electron packet is summarized in Figure 8. The calculated plasma frequency as a function of Earth time corresponding to the position of a 6-keV electron progagating along a smooth Archimedean spiral is given by the upper solid curve in Figure 8. The delay times are Earth-referenced with $t = 0$ to be identified with the onset time for the radio noise storm as observed at Earth. Propagation delays for the radio noise corresponding to the rectilinear paths from the electron positions along the spiral to Earth have been included. Solar wind density and velocity were 5.0 cm^{-3} at 1 AU and 350 km s^{-1}, respectively. The plasma frequency as a function of time for a 6-keV electron with the observed average electron speed along the spiral is given by the upper dashed curve. Observations of the onset times for the type III radio noise as functions of frequency are shown in Figure 8. As noted previously, the

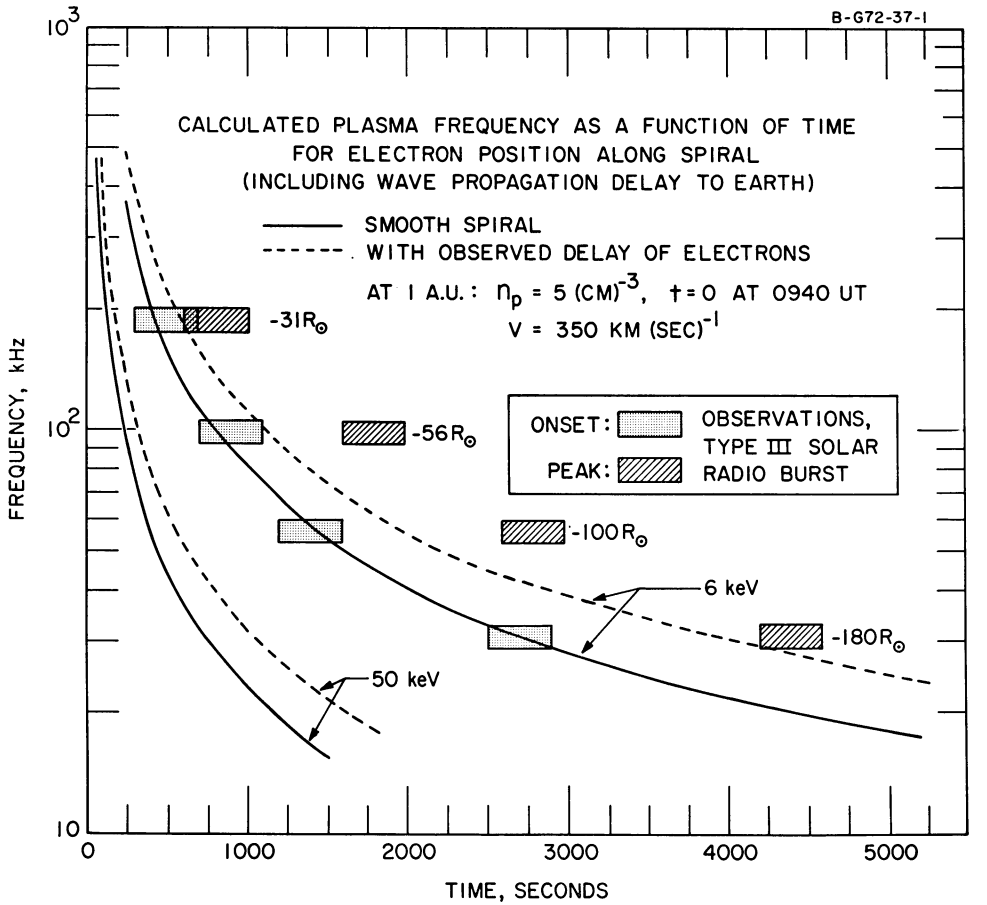

Fig. 8. Electron plasma frequency as a function of time for a 6-keV electron travelling parallel to smooth, Archimedean spiral lines of force (solid line). The abscissa is Earth time since the times for rectilinear light propagation from the positions of the electron along the spiral to Earth have been included. The dashed line represents the plasma frequency as a function of Earth time for the observed average electron speed along the spiral. The corresponding curves for 50-keV electrons also have been included for comparison. Observations of the onset and of first peak intensities for type III radio noise at various frequencies are shown by the shaded blocks. The heights and widths of these blocks represent the filter widths of the frequency spectrum analyzer and our assessment of the accuracy of determining event times, respectively. The time $t = 0$ has been chosen as 0940 UT coincident with the onset of a radio noise storm at centimeter wavelengths as observed at Earth.

low-energy solar electrons in the anisotropic packet are almost certainly the exciting particles for type III radio noise at these low frequencies. The computed heliocentric radial distances corresponding to plasma frequencies 178, 100, 56.6 and 31.1 kHz are 31, 56, 100 and 180 $R_\odot$, respectively. The proximity of the region of 31.1-kHz radio noise generation to the Earth is directly supported by the observed isotropy of intensities at these wavelengths as a function of antenna azimuth. Plasma frequency as a function of time for electrons with energy 50 keV (speed, 0.41c) is given in Figure 8

for comparison with the radio noise measurements and with the results for the lower energy electrons. Again, the solid curve corresponds to propagation along a smooth spiral and the dashed curve reflects the observed delay. The drift rates associated with the 50-keV electrons substantially differ from the observed drift rate of the type III radio burst at these low frequencies.

A comparison of our measurements of type III solar radio bursts at low frequencies with previously reported observations, all of which are at higher frequencies, reveals that the type III radio noise at higher frequencies is generated by electrons with substantially greater energies than 6 keV. The earliest estimates of electron speeds, as deduced by Wild (1950) from determinations of frequency drift rates at ~ 100 MHz, ranged from 0.06–0.3c if the Baumbach-Allen model for the electron densities in the solar corona was assumed. The corresponding range of electron energies is 1–30 keV. However, subsequent determinations of the speeds of the apparent source positions by direction-of-arrival observations indicated a higher range of speeds, 0.2–0.8c (Wild *et al.*, 1959). This higher range of speeds corresponds to electron energies of 10–350 keV. This substantial difference in particle speeds gained with the above two types of measurements was attributed to the generation of type III radio bursts in coronal streamers with electron densities approximately an order of magnitude larger than those used in Wild's earliest estimates. This increased density is reflected in increased electron energies which are calculated from frequency drift rate measurements. By using Newkirk's (1961) model for the electron density in a coronal streamer, Malville (1962) demonstrated that the speeds of the particles associated with type III radio noise generation decreased systematically with decreasing frequency range from 0.45c at 50–180 MHz, to 0.18c at 9–18 MHz. This apparent deceleration of the type III radio noise source with increasing heliocentric radial distances was considered questionable to some extent due to uncertainties in the radial variations of electron densities within the coronal streamers.

More recent satellite observations of frequency drift rates in the lower frequency range 0.7–2.8 MHz have extended these speed determinations outward to heliocentric radial distances of $\sim 30 R_\odot$ (Fainberg and Stone, 1970). These results indicated that the speeds of the noise source average $\sim 0.37c$ in this frequency range and are $\sim 0.47c$ at 1.65–2.8 MHz and $\sim 0.31c$ at 0.70–0.99 MHz. Some evidence of a systematic decrease in these speeds with increasing heliocentric radial distance was also noted in this series of measurements, but this result was considered inconclusive by Fainberg and Stone because of the limited data sample employed in their study.

A survey of the frequency drift rates at low frequencies of ~ 31–178 kHz for a series of observations of type III solar radio bursts with the University of Iowa plasma wave instrument on IMP-6 provides evidence that the frequency drift rate for the radio noise event reported in this paper is more or less typical. As noted earlier the corresponding electron energies are several keV's. These new results indicate that the electron energies corresponding to the excitation of type III radio noise decrease from ~ 40 keV at heliocentric radial distances $\lesssim 0.1$ AU to several keV at ~ 1 AU. The apparent decreasing energy could be the signature of (a) the deceleration of the

solar electrons with increasing heliocentric radial distance as effected, for example, by energy-dependent pitch angle scattering and/or (b) the radial variations of the plasma parameters which control the emission mechanism. The isotropic solar electron intensities following the anisotropic packet may be the direct signature of pitch-angle scattering at <1.0 AU. The control of the interaction energy for electrons by the relevant plasma parameters depends critically upon the generation mechanism for type III radio noise. The present observations of the association of a highly anisotropic solar electron packet with the type III noise excitation, as contrasted to the overall lack of such an association with the isotropic intensities appearing after the arrival of the packet, strongly imply that a coherent plasma instability is responsible for the emission. A possible instability is the two-stream instability as discussed by Gintsburg and Zheleznyakov (1958), rather than an incoherent Cerenkov process which would generate noise levels proportional to the omnidirectional electron intensities.

Our estimates of the electron energies producing the type III radio noise were based upon the widely accepted assumption that this radio noise is generated at or near the electron plasma frequency. However, it is well-known that type III radio noise emissions at higher frequencies $\sim$10–100 MHz, have been observed at both the fundamental (f_{pe}) and the second harmonic ($2f_{pe}$) of the electron plasma frequency (Wild *et al.*, 1954). The mechanism by which the noise is generated at the second harmonic of the electron plasma frequency has been extensively investigated (cf. Gintsburg and Zheleznyakov, 1958; Sturrock, 1961; Tidman *et al.*, 1966; and the review by Kundu, 1965). To our knowledge there is no conclusive experimental evidence that the type III solar radio noise reported here at kilometric wavelengths is generated at the fundamental of the electron plasma frequency, even though this hypothesis is widely accepted by other investigators (cf. Hartz, 1969; Fainberg and Stone, 1971b) for the radio noise observed at the shorter hectometric wavelengths. If our measurements of type III radio noise are in fact those of noise at the second harmonic of the plasma frequency then the electron speeds required to account for the observed frequency dispersion curve of Figure 8 must be increased by a factor of 2. The corresponding electron energy is 25 keV. Although the shape of the frequency dispersion curve would be slightly modified by effects due to the spiral path of the electrons along the interplanetary magnetic field and the propagation times for electromagnetic waves if excitation at the second harmonic is assumed, these effects are not sufficiently large to determine decisively whether the fundamental or its second harmonic is dominant in the radio noise emission. However, we note here that the electron energies of $\sim$25 keV necessary to account for the observed frequency drift rate if emission at the second harmonic peak is assumed are substantially larger than electron energies of $\sim$ several keV corresponding to peak intensities in the anisotropic packet (cf. Figure 6). Furthermore, *peak* intensities of 25-keV electrons are observed with delay times which provide a frequency dispersion curve substantially differing from the measurements of Figure 8. Direction-of-arrival and wide-band measurements of the type III solar radio noise, together with observations of the associated solar electron packets, would be of great value in resolving whether the

fundamental or second harmonic is important in the emission process and in illuminating the mechanism responsible for the apparent deceleration of the solar electrons.

Several theories of type III radio bursts invoke radio noise emission by electrostatic electron plasma oscillations (cf. Gintsburg and Zheleznyakov, 1958; Sturrock, 1961). The question arises naturally here as to whether electron plasma oscillations were detected simultaneously with the arrival of the anisotropic solar electron packet at the spacecraft. The electron density at the spacecraft position was $\sim 5\ \mathrm{cm}^{-3}$, and the corresponding electron plasma frequency was ~ 19.9 kHz. No waves with electric field strengths $\gtrsim 1\ \mu\mathrm{V\ m}^{-1}$, which could be associated with the presence of the anisotropic solar electron packet, were observed with the 16.5 ($\pm 7.5\%$)-kHz channel of the frequency spectrum analyzer. However, it should be pointed out here that sporadic electron plasma oscillations associated with suprathermal electrons streaming away from the Earth's bow shock were observed throughout the entire solar electron event. The sporadic nature of these noise bursts and their close time association with the presence of nonthermal electron intensities from the bow shock provide a clear identification of the origin of these plasma oscillations (Scarf *et al.*, 1971; Fredricks *et al.*, 1971). The absence of detectable electron plasma oscillations in the presence of the anisotropic solar electron packet does not necessarily give reason for immediately rejecting electron plasma oscillations as the mechanism for exciting type III solar radio noise. It is possible that the type III radio noise, and hence the electron plasma oscillations, was not excited at heliocentric radial distances as great as 1 AU during this particular event. The peak noise levels were observed here to decrease with decreasing frequency relatively rapidly from $\sim 40\ \mu\mathrm{V\ m}^{-1}$ in the 178-kHz channel to $\sim 3\ \mu\mathrm{V\ m}^{-1}$ in the 31.1-kHz channel of the frequency spectrum analyzer. Our future studies of these type III solar radio bursts with wide-band coverage of the frequency spectrums, together with simultaneous observations of the solar electron packets, should aid in the clarification of the emission process.

Acknowledgements

We are grateful to Dr K. W. Ogilvie of the Goddard Space Flight Center for generously furnishing us with the solar wind ion densities and velocities for the period of our observations. This research was supported in part by the National Aeronautics and Space Administration under contracts NAS5-11039 and NAS5-11074 and grant NGL16-001-002 and by the Office of Naval Research under contract N000-14-68-A-0196-0003.

References

Anderson, K. A. and Lin, R. P.: 1966, *Phys. Rev. Letters* **16**, 1121.
Anderson, K. A. and Lin, R. P.: 1969, *J. Geophys. Res.* **74**, 3953.
Anderson, K. A., Chase, L. M., Lin, R. P., McCoy, J. E., and McGuire, R. E.: 1971, *Univ. of California (Berkeley) Res. Rep.* **12** (73).
Drake, J. F.: 1971, *Solar Phys.* **16**, 152.

Fainberg, J. and Stone, R. G.: 1970, *Solar Phys.* **15**, 433.
Fainberg, J. and Stone, R. G.: 1971a, *Astrophys. J.* **164**, L123.
Fainberg, J. and Stone, R. G.: 1971b, *Solar Phys.* **17**, 392.
Frank, L. A.: 1967, *J. Geophys. Res.* **72**, 185.
Frank, L. A., Henderson, N. K., and Swisher, R. L.: 1969, *Rev. Sci. Instr.* **40**, 685.
Fredricks, R. W., Scarf, F. L., and Frank, L. A.: 1971, *J. Geophys. Res.* **76**, 6691.
Gintsburg, V. L. and Zheleznyakov, V. V.:1958, *Soviet Astron.* **2**, 653.
Hartz, T. R.: 1969, *Planetary Space Sci.* **17**, 267.
Kundu, M. R.: 1965, *Solar Radio Astronomy*, Interscience Publishers, New York.
Lin, R. P.: 1970, *Solar Phys.* **12**, 266.
Lin, R. P. and Hudson, H. S.: 1971, *Solar Phys.* **17**, 412.
Malville, J. M.: 1962, *Astrophys. J.* **136**, 266.
Montgomery, M. D., Bame, S. J., and Hundhausen, A. J.: 1968, *J. Geophys. Res.* **73**, 4999.
NOAA Solar-Geophysical Data, No. 326, Part II, October 1971.
Newkirk, G.: 1961, *Astrophys. J.* **133**, 983.
Ogilvie, K. W., Scudder, J. D., and Sugiura, M.: 1971, *J. Geophys. Res.* **76**, 8165.
Scarf, F. L., Fredricks, R. W., Frank, L. A., and Neugebauer, M.: 1971, *J. Geophys. Res.* **76**, 5162.
Sturrock, P. A.: 1961, *Nature* **192**, 58.
Tidman, D. A., Birmingham, T. J., and Stainer, H. M.: 1966, *Astrophys. J.* **146**, 207.
Van Allen, J. A.: 1970, *J. Geophys. Res.* **75**, 29.
Van Allen, J. A. and Krimigis, S. M.: 1965, *J. Geophys. Res.* **70**, 5737.
Wild, J. P.: 1950, *Australian J. Sci. Res.* **A3**, 541.
Wild, J. P., Murray, J. D., and Rowe, W. C.: 1954, *Australian J. Phys.* **7**, 439.
Wild, J. P., Sheridan, K. V., and Neylan, A. A.: 1959, *Australian J. Phys.* **12**, 369.